

GEOM: Energy-annotated molecular conformations for property prediction and molecular generation

Simon Axelrod^{1,2} and Rafael Gómez-Bombarelli²

¹Harvard University, Department of Chemistry and Chemical Biology, Cambridge, MA, 02138, USA

²Massachusetts Institute of Technology, Department of Materials Science and Engineering, Cambridge, MA, 02139, USA

*corresponding author: Rafael Gómez-Bombarelli (rafagb@mit.edu)

ABSTRACT

Machine learning (ML) outperforms traditional approaches in many molecular design tasks. ML models usually predict molecular properties from a 2D chemical graph or a single 3D structure, but neither of these representations accounts for the ensemble of 3D conformers accessible to a molecule. Property prediction could be improved by using conformer ensembles as input, but there is no large-scale dataset that contains graphs annotated with high-quality conformers and experimental data. Here we use first-principles simulations to generate accurate conformers for over 430,000 molecules, including 300,000 with experimental data for the inhibition of various pathogens. The Geometric Ensemble Of Molecules (GEOM) dataset contains over 33 million molecular conformers labeled with their relative energies and statistical probabilities at room temperature. GEOM will assist in the development of models that predict properties from conformer ensembles, and generative models that sample 3D conformations.

Background & Summary

Accurate and affordable prediction of molecular properties is a longstanding goal of computational chemistry. Predictions can be generated with rule-based¹ or physics-based² methods, which typically involve a trade-off between accuracy and speed. Machine learning offers an attractive alternative, as it is far quicker than physics-based methods and outperforms traditional rule-based baselines in many molecule-related tasks, including property prediction and virtual screening³⁻⁵, inverse design using generative models⁶⁻¹³, reinforcement learning¹⁴⁻¹⁷, differentiable simulators^{12, 18, 19}, and synthesis planning and retrosynthesis^{20, 21}.

Advances in molecular machine learning have been enabled by algorithmic improvements²²⁻²⁷ and by reference datasets and tasks²⁸. A number of reference datasets provide unlabeled molecules for generation tasks^{7, 29-32} or experimentally labeled molecules for property prediction^{28, 33-36}. The molecules are typically represented as SMILES³⁷ or InChi³⁸ strings, which can be converted into 2D graphs, or as single 3D structures. These representations can be used as input to machine learning models that predict properties or generate new compounds. However, these representations fail to capture the flexibility of molecules, which consist of atoms in continual motion on a potential energy surface. Molecular properties are a function of the conformers accessible at finite temperature^{39, 40}, which are not explicitly included in a 2D or single 3D representation (Fig. 1). Models that map conformer ensembles to experimental properties could be of interest, but they require a dataset with both conformers and experimental data.

Here we present GEOM (Geometric Ensemble Of Molecules), a dataset of high-quality conformers for over 300,000 realistically-sized drug-like molecules with experimental data, and over 130,000 molecules from the QM9 dataset⁴¹. The drug-like species and their experimental properties were accessed as part of AICures⁴², an open machine learning challenge to predict which drugs can be repurposed to treat COVID-19 and related illnesses. Conformers were generated with the CREST program⁴³, which uses extensive sampling based on semi-empirical DFT to generate reliable and accurate structures.

GEOM addresses two key gaps in the dataset literature. First, the data can be used to benchmark new models that take conformers as input to predict experimental properties. Such models could not be trained on the above datasets, which contain only 2D graphs or single 3D structures. Some datasets provide single 3D structures for hundreds of thousands of molecules^{41, 44, 45}, but do not include a full ensemble for each species. Others contain a continuum of high-quality 3D structures for each species, but only contain hundreds of molecules⁴⁶⁻⁵¹. Yet others contain conformers for tens of thousands of molecules with experimental data⁵², but the conformers are of force-field quality (see below). GEOM is unique in its size, number of conformers per species, conformer quality, and connection with experiment.

Second, GEOM can be used to train generative models to predict conformers given an input molecular graph. This is an

active area of research that seeks to lower the computation cost compared to exhaustive torsional approaches and to increase the speed, reliability and accuracy compared stochastic approaches⁵³⁻⁶². The size and simulation accuracy of the GEOM dataset make it an ideal training set. Moreover, machine learning models for conformer generation are orders of magnitude faster than the methods used to generate GEOM. Hence models trained on GEOM may be able to reproduce its accuracy on unseen molecules at a fraction of the cost.

Table 1 provides summary statistics of the molecules that make up the dataset. The drug-like molecules are generally medium-sized organic compounds, containing an average of 44.4 atoms (24.9 heavy atoms), up to a maximum of 181 atoms (91 heavy atoms). They contain a large variance in flexibility, as demonstrated by the mean (6.5) and maximum (53) number of rotatable bonds. 15% (45,712) of the molecules have specified stereochemistry, while 27% (83,326) have stereocenters but may or may not have specified stereochemistry. The QM9 dataset is limited to 9 heavy atoms (29 total atoms), with a much smaller molecular mass and few rotatable bonds. 72% (95,734) of the species have specified stereochemistry.

Table 2 summarizes the experimental properties in the GEOM dataset. Of note is data for the inhibition of SARS-CoV-2, and for the specific inhibition of the SARS-CoV-2 3CL protease. The 3CL protease shares 96% sequence similarity with its SARS-CoV 3CL counterpart⁶³, for which there is significantly more experimental data. The similarity of the two proteases means that CoV-2 models may benefit from pre-training with CoV data, so GEOM can also be used to benchmark transfer learning methods. Another target of interest is the SARS-CoV PL protease^{64,65}. The dataset also contains molecules screened for growth inhibition of *E. Coli* and *Pseudomonas aeruginosa*, both of which can cause secondary infections in COVID-19 patients.

Methods

CREST

Generation of conformers ranked by energy is computationally complex. Many exhaustive, stochastic, and Bayesian methods have been developed to generate conformers⁶⁶⁻⁷³. The exhaustive method is to enumerate all the possible rotations around every bond, but this approach has prohibitive exponential scaling with the number of rotatable bonds^{74,75}. Stochastic algorithms available in cheminformatics packages such as RDKit⁷² suffer from two flaws. First, they explore conformational space very sparsely through a combination of pre-defined distances and stochastic samples⁷⁶ and can miss many low-energy conformations. Second, in most standalone applications conformer energies are determined with classical force fields, which are rather inaccurate⁵¹. As a sampling algorithm, molecular dynamics simulations, in particular metadynamics (MTD) approaches, are somewhat in between: they can sample conformational space more exhaustively but need to evaluate an energy function many times. *Ab initio* methods, such as DFT, can accurately assign energies to conformers more accurately than force fields but are also orders of magnitude more computationally demanding.

An efficient balance between speed and accuracy is offered by the newly developed CREST software⁴³. This program uses semi-empirical tight-binding density functional theory (GFN2-xTB) for energy calculation. The predicted energies are significantly more accurate than classical force fields, accounting for electronic effects, rare functional groups, and bond-breaking/formation of labile bonds, but are computationally less demanding than full DFT. Moreover, the search algorithm is based on MTD, a well-established thermodynamic sampling approach that can efficiently explore the low-energy search space. Finally, the CREST software identifies and groups rotamers, conformers that are identical except for atom re-indexing. It then assigns each conformer a probability through $p_i = d_i \exp(-E_i/k_B T) / \sum_j d_j \exp(-E_j/k_B T)$. Here p_i is the statistical weight of the i^{th} conformer, d_i is its degeneracy (i.e., how many chemically and permutationally equivalent rotamers correspond to the same conformer), E_i is its energy, k_B is the Boltzmann constant, T is the temperature, and the sum is over all conformers. The accurate identification of probabilities is unique to CREST. Methods with low-cost force fields are not accurate enough to assign energies, and degeneracies cannot be accounted for without identifying rotamers.

To generate conformers and rotamers, CREST takes a geometry as input and uses its flexibility to determine an MTD simulation time t_{max} (between 5 and 200 ps). The initial structure is deformed by propagating Newton's equations of motion with an NVT thermostat⁷⁷ from time $t = 0$ to t_{max} . The potential at each time step is given by the sum of the GFN2-xTB potential energy and a bias potential,

$$V_{\text{bias}} = \sum_i^n k_i \exp(-\alpha_i \Delta_i^2), \quad (1)$$

which forces the molecule into new conformations. The collective variables Δ_i are the root-mean-square displacements (RMSDs) of the structure with respect to the i^{th} reference structure, n is the number of reference structures, k_i is the pushing strength and α_i determines the potentials' shapes. A new reference structure from the trajectory is added to V_{bias} every 1.0 ps, driving the molecule to explore new conformations. Different molecules require different (k_i, α_i) pairs to produce best results, so twelve different MTD runs are used with different settings for the V_{bias} parameters.

Geometries from the MTD runs are then optimized with GFN2-xTB. Conformers are identified as structures with $\Delta E > E_{\text{thr}}$, $\text{RMSD} > \text{RMSD}_{\text{thr}}$, and $\Delta B_e > B_{\text{thr}}$, where ΔE is the energy difference between structures, ΔB_e is the difference in their rotational constants, and thr denotes a threshold value. Rotamers are identified through $\Delta E < E_{\text{thr}}$, $\text{RMSD} > \text{RMSD}_{\text{thr}}$, and $\Delta B_e < B_{\text{thr}}$. Duplicates are identified through $\Delta E < E_{\text{thr}}$, $\text{RMSD} < \text{RMSD}_{\text{thr}}$, and $\Delta B_e < B_{\text{thr}}$. The defaults, which are used in this work, are $E_{\text{thr}} = 0.1$ kcal/mol, $\text{RMSD}_{\text{thr}} = 0.125$ Å, and $B_{\text{thr}} = 15.0$ MHz. Conformers and rotamers are added to the conformer-rotamer ensemble (CRE) and duplicates are discarded.

If a new conformer has a lower energy than the input structure, the procedure is restarted using the conformer as input, and the resulting structures are added to the CRE. The procedure is restarted between one and five times. The three conformers of lowest energy then undergo two normal molecular dynamics (MD) simulations at 400K and 500K. These are used to sample low-energy barrier crossings, such as simple torsional motions, which are needed to identify the remaining rotamers. Conformers and rotamers are once again identified and added to the CRE. All accumulated structures are then used as inputs to a genetic Z-matrix crossing algorithm^{77,78}, the results of which are also added to the CRE. All geometries accumulated throughout the sampling process are optimized with a tight convergence threshold, identified as conformers, rotamers or duplicates, and sorted to yield the final set of structures. The process is restarted after the regular MD runs or the tight optimization if any conformers have lower energy than the input, with no limit to the number of restarts.

The final CRE contains conformers and rotamers up to a maximum energy E_{win} . The default $E_{\text{win}} = 6.0$ kcal/mol provides a safety net around errors in the xTB energies, as only conformers with $E \lesssim 2.0$ kcal/mol have significant population at room temperature.

Conformer generation

SMILES pre-processing of drug-like molecules

SMILES strings and properties of the drug-like molecules were accessed from Refs.^{79,80} (original sources are^{3,64,65,80-85}). Each SMILES string was converted to its canonical form using RDKit. This allowed us to assign multiple properties from multiple sources to a single species, even if different non-canonical SMILES strings were used in the original sources.

3.9% of the drug molecules accessed (11,886 total) were given as clusters, either with a counterbalancing ion (e.g. “[Na+]”, “[Cl-]”) or with an acid to represent the protonated salt (e.g. “.Cl”). For non acid-base clusters we identified the compound of interest as the heaviest component of the cluster. For the acid/base SMILES strings, used reaction SMARTS in RDKit to generate the protonated molecule and counterion. This product SMILES was used in place of the original SMILES. Original SMILES strings are available in the dataset with the key `uncleaned_smiles` (see Ref.⁸⁶ for details). Not only does de-salting identify the drug-like compound in each cluster and correct its ionization state, it also homogenizes the molecular representations in the drug datasets.

Initial structure generation

To generate conformers with CREST one must provide an initial guess geometry, ideally optimized at the same level of theory as the simulation (GFN2-xTB). For the drug molecules we therefore used RDKit to generate initial conformers from SMILES strings, optimized each conformer with GFN2-xTB, and used the lowest energy conformer as input to CREST.

Conformers were generated in RDKit using the `EmbedMultipleConfs` command with 50 conformers (`numConfs = 50`), a pruning threshold of similar conformers of 0.01 Å (`pruneRmsThresh = 0.01`), a maximum of five embedding attempts per conformer (`maxAttempts = 5`), coordinate initialization from the eigenvalues of the distance matrix (`useRandomCoords = False`), and a random seed. If no conformers were successfully generated then `numConfs` was increased to 500. Each conformer was then optimized with the MMFF force field⁸⁷ in RDKit using the default arguments. Duplicate conformers, identified as those with an RMSD below 0.1 Å, were removed after optimization. Optimization was skipped for any molecules with *cis/trans* stereochemistry (indicated by “\” or “/” in the SMILES string), as such stereochemistry is not always maintained during RDKit optimization.

The ten MMFF-optimized conformers with the lowest energy were further optimized with xTB using Orca 4.2.0^{88,89}. The conformer with the lowest xTB energy was selected as the seed geometry for CREST. The QM9 molecules are already optimized with DFT, and so in principle did not need to be optimized further for CREST. However, since it is recommended to seed CREST with a structure optimized at the GFN2-xTB level of theory, we re-optimized each QM9 geometry with xTB before using it in CREST.

CREST simulation

A single xTB-optimized structure was used as input to the CREST simulation of each species. Default values were used for all CREST arguments, except for the charge of each geometry. CREST runs on the drug dataset took an average of 2.8 hours of wall time on 32 cores on Knights Landing (KNL) nodes (89.1 core hours), and 0.63 hours on 13 cores on Cascade Lake and Sky Lake nodes (8.2 core hours). QM9 jobs were only performed on the latter two nodes, and took an average of 0.04 wall hours on 13 cores (0.5 core hours). 13 million KNL core hours and 1.2 million Cascade Lake/Sky Lake core hours were used in total.

Graph re-identification

It was necessary to re-identify the graph of each conformer generated by CREST, for the following reasons. First, stereochemistry may not have been specified in the original SMILES string, but necessarily existed in each of the generated 3D structures. Second, reactivity such as dissociation or tautomerization may have occurred in the CREST simulations (CREST has specific commands to generate tautomers, but they were not used here). This would also lead to conformers with different graphs.

To re-identify the graphs we used `xyz2mol`⁹⁰ (code accessed from⁹¹) to generate an RDKit `mol` object. These `mol` objects were used to assign graph features to each conformer (see Data Records). It should be noted that `xyz2mol` sometimes assigned resonance structure graphs instead of the original graphs. In some cases this caused different conformers of the same species to have different graphs. This happened, for example, when the conformers had different *cis/trans* isomerism about a double bond that was only present because of the resonance structure used (see the RDKit tutorial in Ref.⁸⁶). This is conceptually different from species whose conformer graphs differ because of reactivity. One may want to distinguish these two cases when analyzing the conformer `mol` objects.

Conformational property prediction

The GEOM dataset is significant because it allows for the training of conformer-based property predictors and generative models to predict new conformations. The first application will be explored in a future publication⁹². The second application is necessary for using conformer-based ML models in practice, since generating CREST structures from scratch is too costly for the virtual screening of new species. Such work is already underway⁹³, paving the way for `graph` \rightarrow `conformer ensemble` \rightarrow `property` models that can be trained end-to-end. Here we give an example of a simpler application in the same vein, benchmarking methods to predict *summary statistics* of each conformer ensemble, rather than the conformers themselves. Our proposed tasks are similar to the benchmark QM9 tasks, which measure a model’s ability to predict properties that are uniquely determined by geometry. Here, since we provide conformer ensembles for each species, we measure a model’s ability to predict properties defined by the ensemble. Because one chemical graph spawns a unique conformer ensemble, these tasks are also a metric of the performance of graph-based models to infer properties mediated through conformational flexibility.

We trained different models to predict three quantities related to conformational information. A summary of these quantities can be found in Table 2 and Fig. 3. The first quantity is the conformational free energy, $G = -TS$, where the ensemble entropy is $S = -R\sum_i p_i \log p_i$ ⁴³. Here the sum is over the statistical probabilities p_i of the i^{th} conformer, and R is the gas constant. The conformational entropy is a measure of the conformational degrees of freedom available to a molecule. A molecule with only one conformer has an entropy of exactly 0, while a molecule with equal statistical weight for an infinite number of conformers has infinite conformational entropy. The conformational Gibbs free energy is an important quantity for predicting the binding affinity of a drug to a target. The affinity is determined by the change in Gibbs free energy of the molecule and protein upon binding, which includes the loss of molecular conformational free energy⁹⁴. The second quantity is the average conformational energy. The average energy is given by $\langle E \rangle = \sum_i p_i E_i$, where E_i is the energy of the i^{th} conformer. Each energy is defined with respect to the lowest-energy conformer. The third quantity is the number of unique conformers for a given molecule, as predicted by CREST within the default maximum energy window⁴³.

We trained a kernel ridge regression (KRR) model⁹⁵, a random forest⁹⁶, and three different neural networks to predict conformer properties. The random forest, KRR and feed-forward neural network (FFNN) models were trained on Morgan fingerprints⁹⁷ generated through RDKit. Two different message-passing neural networks⁹⁸ were trained. The first, called ChemProp, has achieved state-of-the-art performance on a number of benchmarks⁹⁹. The second is based on the SchNet force field model^{100,101}. We call it SchNetFeatures, as it learns from 3D geometries using the SchNet architecture, but also incorporates graph-based node and bond features. The SchNetFeatures models were trained on the highest-probability conformer of each species.

100,000 species were sampled randomly from the drug subset of GEOM dataset. We used the same 60-20-20 train-validation-test split for each model. The splits, trained models, and log files can be found with the GEOM dataset at¹⁰², under the heading “synthetic”. Hyperparameters were optimized for each model type and for each task using the hyperopt package¹⁰³. Details of the hyperparameter searches, optimal parameters, and network architectures can be found in¹⁰². Source code is available at¹⁰⁴.

Results are shown in Table 3. ChemProp and SchNetFeatures are the strongest models overall, followed in order by FFNN, KRR, and random forest. Of the three models that use fixed 2D fingerprints, we see that the FFNN is best able to map these non-learnable representations to properties. ChemProp has the added flexibility of learning an ideal molecular representation directly from the graph, and so performs even better than the FFNN. The SchNetFeatures model retains this flexibility while incorporating extra information from one 3D structure. Compared to ChemProp, its prediction error is 10% lower for G , nearly equal for $\langle E \rangle$, and 5% lower for $\ln(\text{unique conformers})$. This is not surprising, as the ensemble properties are mainly determined by molecular flexibility, which is a function of the graph through the number of rotatable bonds. A single 3D geometry would not provide extra information about this flexibility.

We see that various models can accurately predict conformer properties when trained on the GEOM dataset. With access to the dataset, researchers will therefore be able to predict results of expensive simulations without performing them directly. This has implications beyond ensemble-averaged properties, as generative models trained on the GEOM dataset will also be able to produce the conformers themselves⁹³.

Data Records

The dataset is available online at¹⁰⁵, and detailed tutorials for loading the data can be found at⁸⁶.

The data is available either through MessagePack¹⁰⁶, a language-agnostic binary serialization format, or through Python pickle files. There are two MessagePack files for the drug dataset and two for QM9. Each of the two files contains a dictionary, where the keys are SMILES strings and the values are sub-dictionaries. In the file with suffix `crude`, the sub-dictionaries contain both species-level information (experimental binding data, average conformer energy, etc.) and a list of dictionaries for each conformer. Each conformer dictionary has its own conformer-level information (geometry, energy, degeneracy, etc.). In the file with suffix `featurized`, each conformer dictionary contains information about its molecular graph.

The Python pickle files are organized in a different fashion. The main folder is divided into QM9 and drug sub-folders, each of which contains one pickle file for each species. Each pickle file contains both summary information and conformer information for its species. Each conformer is stored as an RDKit `mol` object, so that it contains both the geometry and graph features. One may only want to load the pickle files of species with specific properties (e.g., those with experimental data for SARS-CoV-2 inhibition); for this one can use the summary `JSON` file. This file contains all summary information along with the path to the pickle file, but without the list of conformers. It is therefore lightweight and quick to load, and can be used to choose species before loading their pickles.

Technical Validation

The quality of the data was validated in four different ways. First, we checked that the conformer data was accurately parsed from the CREST calculations. To do so we randomly sampled one conformer from 20 different species and manually confirmed that its data matched the data in the CREST output files.

Second, we re-identified the graphs of the conformers generated by CREST using `xyz2mol`. The graph re-attribution procedure succeeded for 88.4% of the QM9 molecules and 94.7% of the drug molecules, recovering the original molecular graph that was used to generate each conformer. Note that to compare graphs we removed stereochemical indicators from the original and the re-generated graph. This was done because of cases in which stereochemistry was not specified originally but was specified in the generated conformers. All of the failed QM9 graphs underwent some sort of reaction, which can be explained by the presence of highly strained and unstable molecules. However, manual inspection of 53 cases in the drug dataset suggests that 70% of the drug graphs failed only because of poor handling of resonance forms by `xyz2mol` (see above). This means that the original graph was likely recovered for 98.4% of all drugs. 21% of cases failed because of tautomerization (1% of all cases), and 9.4% failed because of a different reaction (usually dissociation or ring formation; 0.5% of all cases). The high success rate of the graph re-identification indicates that, in the vast majority of cases, the geometries generated by CREST were actual conformers of the species.

Third, we compared the geometries generated by CREST with geometries refined at higher levels of theory and verified that they were reasonably well-correlated. We sampled 100 different species with less than 50 total atoms, and from each species we selected the highest-probability conformer plus two random conformers of higher energy, for a total of 300 geometries. Each conformer was then optimized with DFT using Orca 4.2.0^{88,89}, first with the BP86-D3 functional^{107,108,108,109} and the def2-SVP basis¹¹⁰, and then with the more accurate wb97X-D3 functional^{109,111} and the larger def2-TZVP basis¹¹⁰. To compare conformers that were optimized at different levels of theory we first aligned the structures using the quaternion algorithm¹¹². The RMSD between each pair of conformers was then calculated as $(\sum_{i=1}^N \sum_{\alpha=1}^3 (\vec{r}_{i\alpha}^A - \vec{r}_{i\alpha}^B)^2 / N)^{1/2}$, where N is the number of atom in each molecule, $\vec{r}_{i\alpha}^A$ is the position of atom i in direction α computed at level of theory A , and $\vec{r}_{i\alpha}^B$ is the corresponding coordinate at level of theory B . Results are shown in Fig. 4(a) and (b). The median RMSD between xTB and BP86 geometries is 0.23 Å, and the mean is 0.41 Å. The median RMSD indicates good agreement between the two sets of geometries. The mean is significantly higher than the median because of outliers with high RMSDs. The median RMSD between xTB and wb97X geometries is 0.64 Å, and the mean is 0.75 Å. These values indicate more significant disagreement but are still reasonable.

Lastly we evaluated the reliability of the xTB energies. To do so we re-optimized each conformer at a higher level of theory and calculated the corresponding energy. The lowest energy of each species was then subtracted, giving the relative energy of each conformer. Each relative energy was compared with the CREST-computed relative energy of the original conformer. Results are shown in Fig. 4(c) and (d). Panels (e) and (f) show the same results but excluding the xTB geometries of lowest energy. There is fairly good correlation between xTB and BP86 results. The coefficient of determination, R^2 , is 0.70 when

including all conformers and 0.58 when excluding the lowest energy structures. The corresponding errors are 0.93 kcal/mol and 1.26 kcal/mol, respectively. The error is higher when excluding the lowest-energy structures because, by definition, the relative energy of each such structure is 0 if it is at the global minimum of the potential energy surface. The error is higher for wB97X than for BP86, with R^2 values of 0.53 and 0.42 and MAE values of 1.05 and 1.37 kcal/mol. We see that the CREST conformer energies are fairly well-correlated with BP86 results, and somewhat correlated with wb97X results.

Usage Notes

Researchers are encouraged to use the data-loading tutorials given in⁸⁶. We suggest loading the data through the RDKit pickle files, as RDKit `mol` objects are easy to handle and their properties can be readily analyzed. The MessagePack files, while secure and accessible in all languages, represent graphs through their features rather than objects with built-in methods, and are thus more difficult to analyze. To train 3D-based models we suggest following the tutorial and README file in¹⁰⁴.

Code availability

Tutorials for loading the dataset⁸⁶ and code for training 3D-based neural network models¹⁰⁴ are publicly available without restriction. CREST¹¹³ and xTB¹¹⁴ are both freely available online. CREST version 2.9 and xTB version 6.2.3 were used in this work.

References

1. Norinder, U., Lidén, P. & Boström, H. Discrimination between modes of toxic action of phenols using rule based methods. *Molecular diversity* **10**, 207–212 (2006).
2. Durrant, J. D. & McCammon, J. A. Molecular dynamics simulations and drug discovery. *BMC biology* **9**, 1–9 (2011).
3. Stokes, J. M. *et al.* A deep learning approach to antibiotic discovery. *Cell* **180**, 688–702 (2020).
4. Gómez-Bombarelli, R. *et al.* Design of efficient molecular organic light-emitting diodes by a high-throughput virtual screening and experimental approach. *Nature Materials* **15**, 1120–1127, [10.1038/nmat4717](https://doi.org/10.1038/nmat4717) (2016).
5. Zhavoronkov, A. *et al.* Deep learning enables rapid identification of potent DDR1 kinase inhibitors. *Nature biotechnology* **37**, 1038–1040, [10.1038/s41587-019-0224-x](https://doi.org/10.1038/s41587-019-0224-x) (2019).
6. Schwalbe-Koda, D. & Gómez-Bombarelli, R. Generative Models for Automatic Chemical Design. *arXiv:1907.01632* (2019). [1907.01632](https://arxiv.org/abs/1907.01632).
7. Gómez-Bombarelli, R. *et al.* Automatic Chemical Design Using a Data-Driven Continuous Representation of Molecules. *ACS Central Science* **4**, 268–276, [10.1021/acscentsci.7b00572](https://doi.org/10.1021/acscentsci.7b00572) (2018). [1610.02415](https://arxiv.org/abs/1610.02415).
8. Jin, W., Barzilay, R. & Jaakkola, T. Junction Tree Variational Autoencoder for Molecular Graph Generation. In *Proceedings of the 35th International Conference on Machine Learning*, [1802.04364v2](https://arxiv.org/abs/1802.04364v2) (2018). [1802.04364](https://arxiv.org/abs/1802.04364).
9. De Cao, N. & Kipf, T. MolGAN: An implicit generative model for small molecular graphs. *arXiv:1805.11973* [arXiv:1805.11973v1](https://arxiv.org/abs/1805.11973v1) (2018). [1805.11973](https://arxiv.org/abs/1805.11973).
10. Li, Y., Vinyals, O., Dyer, C., Pascanu, R. & Battaglia, P. Learning Deep Generative Models of Graphs. *arXiv:1803.03324* [arXiv:1803](https://arxiv.org/abs/1803.03324), [10.1146/annurev-statistics-010814-020120](https://arxiv.org/abs/10.1146/annurev-statistics-010814-020120) (2018). [1803.03324](https://arxiv.org/abs/1803.03324).
11. Dai, H., Tian, Y., Dai, B., Skiena, S. & Song, L. Syntax-Directed Variational Autoencoder for Structured Data. *arXiv:1802.08786* (2018). [1802.08786](https://arxiv.org/abs/1802.08786).
12. Wang, W., Axelrod, S. & Gómez-Bombarelli, R. Differentiable molecular simulations for control and learning. *arXiv preprint arXiv:2003.00868* (2020).
13. Noé, F., Olsson, S., Köhler, J. & Wu, H. Boltzmann generators: Sampling equilibrium states of many-body systems with deep learning. *Science* **365**, eaaw1147, [10.1126/science.aaw1147](https://doi.org/10.1126/science.aaw1147) (2019). [1812.01729](https://arxiv.org/abs/1812.01729).
14. Olivecrona, M., Blaschke, T., Engkvist, O. & Chen, H. Molecular De Novo Design through Deep Reinforcement Learning. *arXiv:1704.07555* [10.1186/s13321-017-0235-x](https://doi.org/10.1186/s13321-017-0235-x) (2017). [1704.07555](https://arxiv.org/abs/1704.07555).
15. Gottipati, S. K. *et al.* Learning to navigate the synthetically accessible chemical space using reinforcement learning. *arXiv preprint arXiv:2004.12485* (2020).
16. Guimaraes, G. L., Sanchez-Lengeling, B., Outeiral, C., Farias, P. L. C. & Aspuru-Guzik, A. Objective-Reinforced Generative Adversarial Networks (ORGAN) for Sequence Generation Models. *arXiv:1705.10843* (2017). [1705.10843](https://arxiv.org/abs/1705.10843).

17. Popova, M., Isayev, O. & Tropsha, A. Deep reinforcement learning for de novo drug design. *Science Advances* **4**, eaap7885, [10.1126/sciadv.aap7885](https://doi.org/10.1126/sciadv.aap7885) (2018).
18. AlQuraishi, M. End-to-End Differentiable Learning of Protein Structure. *Cell Systems* [10.1016/J.CELS.2019.03.006](https://doi.org/10.1016/j.cels.2019.03.006) (2019).
19. Ingraham, J., Riesselman, A., Sander, C. & Marks, D. Learning Protein Structure with a Differentiable Simulator. In *International Conference on Learning Representations* (2019).
20. Segler, M. H. S., Preuss, M. & Waller, M. P. Planning chemical syntheses with deep neural networks and symbolic {AI}. *Nature* **555**, 604–610, [10.1038/nature25978](https://doi.org/10.1038/nature25978) (2018).
21. Coley, C. W., Barzilay, R., Jaakkola, T. S., Green, W. H. & Jensen, K. F. Prediction of Organic Reaction Outcomes Using Machine Learning. *ACS Central Science* **3**, 434–443, [10.1021/acscentsci.7b00064](https://doi.org/10.1021/acscentsci.7b00064) (2017).
22. Duvenaud, D. K. *et al.* Convolutional Networks on Graphs for Learning Molecular Fingerprints. In *Advances in Neural Information Processing Systems*, 2215–2223 (2015). [1509.09292v2](https://arxiv.org/abs/1509.09292v2).
23. Kearnes, S., McCloskey, K., Berndl, M., Pande, V. & Riley, P. Molecular graph convolutions: moving beyond fingerprints. *Journal Computer-Aided Molecular Design* **30**, 595–608, [10.1007/s10822-016-9938-8](https://doi.org/10.1007/s10822-016-9938-8) (2016). [1603.00856](https://doi.org/10.1007/s10822-016-9938-8).
24. Yang, K. *et al.* Analyzing Learned Molecular Representations for Property Prediction. *Journal Chemical Information Modeling* **59**, 3370–3388, [10.1021/acs.jcim.9b00237](https://doi.org/10.1021/acs.jcim.9b00237) (2019). [1904.01561](https://arxiv.org/abs/1904.01561).
25. Anderson, B., Hy, T. S. & Kondor, R. Cormorant: Covariant molecular neural networks. In *Advances in Neural Information Processing Systems*, 14537–14546 (2019).
26. Thomas, N. *et al.* Tensor field networks: Rotation-and translation-equivariant neural networks for 3d point clouds. *arXiv preprint arXiv:1802.08219* (2018).
27. Klicpera, J., Groß, J. & Günnemann, S. Directional message passing for molecular graphs. In *International Conference on Learning Representations* (2019).
28. Ramsundar, B. *et al.* *Deep Learning for the Life Sciences* (O'Reilly Media, 2019). <https://www.amazon.com/Deep-Learning-Life-Sciences-Microscopy/dp/1492039837>.
29. Mendez, D. *et al.* ChEMBL: towards direct deposition of bioassay data. *Nucleic Acids Research* **47**, D930–D940, [10.1093/nar/gky1075](https://doi.org/10.1093/nar/gky1075) (2018). <https://academic.oup.com/nar/article-pdf/47/D1/D930/27437436/gky1075.pdf>.
30. Sterling, T. & Irwin, J. J. ZINC 15–Ligand Discovery for Everyone. *Journal chemical information modeling* **55**, 2324–37, [10.1021/acs.jcim.5b00559](https://doi.org/10.1021/acs.jcim.5b00559) (2015).
31. Brown, N., Fiscato, M., Segler, M. H. S. & Vaucher, A. C. {GuacaMol}: Benchmarking Models for de Novo Molecular Design. *J. Chem. Inf. Model.* **59**, 1096–1108 (2019).
32. Polykovskiy, D. *et al.* Molecular Sets (MOSES): A Benchmarking Platform for Molecular Generation Models. *arXiv:1811.12823* (2018).
33. Delaney, J. S. ESOL: Estimating aqueous solubility directly from molecular structure. *Journal Chemical Information Computer Sciences* **44**, 1000–1005, [10.1021/ci034243x](https://doi.org/10.1021/ci034243x) (2004).
34. Mobley, D. L. & Guthrie, J. P. FreeSolv: A database of experimental and calculated hydration free energies, with input files. *Journal Computer-Aided Molecular Design* **28**, 711–720, [10.1007/s10822-014-9747-x](https://doi.org/10.1007/s10822-014-9747-x) (2014).
35. Wang, R., Fang, X., Lu, Y. & Wang, S. The PDBbind database: Collection of binding affinities for protein-ligand complexes with known three-dimensional structures. *Journal Medicinal Chemistry* **47**, 2977–2980, [10.1021/jm0305801](https://doi.org/10.1021/jm0305801) (2004).
36. Wu, Z. *et al.* {MoleculeNet}: a benchmark for molecular machine learning. *Chem. Sci.* **9**, 513–530 (2018).
37. Weininger, D. SMILES, a chemical language and information system. 1. Introduction to methodology and encoding rules. *Journal Chemical Information Modeling* **28**, 31–36, [10.1021/ci00057a005](https://doi.org/10.1021/ci00057a005) (1988).
38. Heller, S. R., McNaught, A., Pletnev, I., Stein, S. & Tchekhovskoi, D. InChI, the IUPAC International Chemical Identifier. *Journal cheminformatics* **7**, 23, [10.1186/s13321-015-0068-4](https://doi.org/10.1186/s13321-015-0068-4) (2015).
39. Kuhn, B. *et al.* A real-world perspective on molecular design: Miniperspective. *Journal medicinal chemistry* **59**, 4087–4102 (2016).
40. Hawkins, P. C. Conformation generation: the state of the art. *Journal chemical information modeling* **57**, 1747–1756 (2017).

41. Ramakrishnan, R., Dral, P. O., Rupp, M. & von Lilienfeld, O. A. Quantum chemistry structures and properties of 134 kilo molecules. *Scientific data* **1**, 140022, [10.1038/sdata.2014.22](https://doi.org/10.1038/sdata.2014.22) (2014).
42. Home | AI Cures.
43. Grimme, S. Exploration of chemical compound, conformer, and reaction space with meta-dynamics simulations based on tight-binding quantum chemical calculations. *Journal chemical theory computation* **15**, 2847–2862 (2019).
44. Gražulis, S. *et al.* Crystallography open database—an open-access collection of crystal structures. *Journal applied crystallography* **42**, 726–729 (2009).
45. Groom, C. R., Bruno, I. J., Lightfoot, M. P. & Ward, S. C. The cambridge structural database. *Acta Crystallographica Section B: Structural Science, Crystal Engineering Materials* **72**, 171–179 (2016).
46. Smith, J. S., Isayev, O. & Roitberg, A. E. ANI-1, A data set of 20 million calculated off-equilibrium conformations for organic molecules. *Scientific Data* **4**, 170193, [10.1038/sdata.2017.193](https://doi.org/10.1038/sdata.2017.193) (2017).
47. Smith, J. S., Isayev, O. & Roitberg, A. E. ANI-1: an extensible neural network potential with DFT accuracy at force field computational cost. *Chemical Science* **8**, 3192–3203, [10.1039/C6SC05720A](https://doi.org/10.1039/C6SC05720A) (2017). [1610.08935](https://doi.org/10.1039/C6SC05720A).
48. Smith, J. S., Nebgen, B., Lubbers, N., Isayev, O. & Roitberg, A. E. Less is more: Sampling chemical space with active learning. *Journal Chemical Physics* **148**, 241733, [10.1063/1.5023802](https://doi.org/10.1063/1.5023802) (2018). [1801.09319](https://doi.org/10.1063/1.5023802).
49. Chmiela, S. *et al.* Machine learning of accurate energy-conserving molecular force fields. *Science Advances* **3**, e1603015, [10.1126/sciadv.1603015](https://doi.org/10.1126/sciadv.1603015) (2017).
50. Simm, G. N. & Hernández-Lobato, J. M. A generative model for molecular distance geometry. *arXiv preprint arXiv:1909.11459* (2019).
51. Kanal, I. Y., Keith, J. A. & Hutchison, G. R. A sobering assessment of small-molecule force field methods for low energy conformer predictions. *International Journal Quantum Chemistry* **118**, e25512, [10.1002/qua.25512](https://doi.org/10.1002/qua.25512) (2018).
52. Bolton, E. E., Kim, S. & Bryant, S. H. Pubchem3d: conformer generation. *Journal cheminformatics* **3**, 4 (2011).
53. Hoffmann, J. *et al.* Data-driven approach to encoding and decoding 3-d crystal structures. *arXiv preprint arXiv:1909.00949* (2019).
54. Simm, G. N., Pinsler, R. & Hernández-Lobato, J. M. Reinforcement learning for molecular design guided by quantum mechanics. *arXiv preprint arXiv:2002.07717* (2020).
55. Stieffenhofer, M., Wand, M. & Berau, T. Adversarial reverse mapping of equilibrated condensed-phase molecular structures. *arXiv preprint arXiv:2003.07753* (2020).
56. Hoffmann, M. & Noé, F. Generating valid euclidean distance matrices. *arXiv preprint arXiv:1910.03131* (2019).
57. Imrie, F., Bradley, A. R., van der Schaar, M. & Deane, C. M. Deep Generative Models for 3D Linker Design. *Journal chemical information modeling* **60**, 1983–1995, [10.1021/acs.jcim.9b01120](https://doi.org/10.1021/acs.jcim.9b01120) (2020).
58. Mansimov, E., Mahmood, O., Kang, S. & Cho, K. Molecular Geometry Prediction using a Deep Generative Graph Neural Network. *Scientific Reports* **9**, 1–13, [10.1038/s41598-019-56773-5](https://doi.org/10.1038/s41598-019-56773-5) (2019). [1904.00314](https://doi.org/10.1038/s41598-019-56773-5).
59. Chan, L., Hutchison, G. R. & Morris, G. M. Bayesian optimization for conformer generation. *Journal Cheminformatics* **11**, 32, [10.1186/s13321-019-0354-7](https://doi.org/10.1186/s13321-019-0354-7) (2019).
60. Gebauer, N. W. A., Gastegger, M. & Schütt, K. T. Symmetry-adapted generation of 3d point sets for the targeted discovery of molecules. *arXiv:1906.00957* (2019). [1906.00957](https://doi.org/10.1101/1906.00957).
61. Gebauer, N. W. A., Gastegger, M. & Schütt, K. T. Generating equilibrium molecules with deep neural networks. *arXiv:1810.11347* (2018). [1810.11347](https://doi.org/10.1101/1810.11347).
62. Wang, W. & Gómez-Bombarelli, R. Coarse-graining auto-encoders for molecular dynamics. *npj Computational Materials* **5**, 125, [10.1038/s41524-019-0261-5](https://doi.org/10.1038/s41524-019-0261-5) (2019).
63. Xu, Z. *et al.* Nelfinavir was predicted to be a potential inhibitor of 2019-ncov main protease by an integrative approach combining homology modelling, molecular docking and binding free energy calculation. *BioRxiv* (2020).
64. Engel, D. qHTS of yeast-based assay for SARS-CoV PLP. <https://pubchem.ncbi.nlm.nih.gov/bioassay/485353>.
65. Engel, D. qHTS of yeast-based assay for SARS-CoV PLP: Hit validation. <https://pubchem.ncbi.nlm.nih.gov/bioassay/652038>.
66. Vainio, M. J. & Johnson, M. S. Generating conformer ensembles using a multiobjective genetic algorithm. *Journal chemical information modeling* **47**, 2462–2474 (2007).

67. Puranen, J. S., Vainio, M. J. & Johnson, M. S. Accurate conformation-dependent molecular electrostatic potentials for high-throughput in silico drug discovery. *Journal computational chemistry* **31**, 1722–1732 (2010).
68. O'Boyle, N. M., Vandermeersch, T., Flynn, C. J., Maguire, A. R. & Hutchison, G. R. Confab-Systematic generation of diverse low-energy conformers. *Journal cheminformatics* **3**, 1–9 (2011).
69. Miteva, M. A., Guyon, F. & Pierre, T. Frog2: Efficient 3D conformation ensemble generator for small compounds. *Nucleic acids research* **38**, W622–W627 (2010).
70. ULC, C. C. G. CCG: Molecular Operating Environment (MOE). <http://www.chemcomp.com/> (2018).
71. Hawkins, P. C., Skillman, A. G., Warren, G. L., Ellingson, B. A. & Stahl, M. T. Conformer generation with OMEGA: algorithm and validation using high quality structures from the Protein Databank and Cambridge Structural Database. *Journal chemical information modeling* **50**, 572–584 (2010).
72. RDKit: Open-source cheminformatics. <http://www.rdkit.org>.
73. Chan, L., Hutchison, G. R. & Morris, G. M. Bayesian optimization for conformer generation. *Journal cheminformatics* **11**, 1–11 (2019).
74. Schwab, C. H. Conformations and 3D pharmacophore searching, [10.1016/j.ddtec.2010.10.003](https://doi.org/10.1016/j.ddtec.2010.10.003) (2010).
75. O'Boyle, N. M., Vandermeersch, T., Flynn, C. J., Maguire, A. R. & Hutchison, G. R. Confab - Systematic generation of diverse low-energy conformers. *Journal Cheminformatics* **3**, 8, [10.1186/1758-2946-3-8](https://doi.org/10.1186/1758-2946-3-8) (2011).
76. Spellmeyer, D. C., Wong, A. K., Bower, M. J. & Blaney, J. M. Conformational analysis using distance geometry methods. *Journal Molecular Graphics Modelling* **15**, 18–36, [10.1016/S1093-3263\(97\)00014-4](https://doi.org/10.1016/S1093-3263(97)00014-4) (1997).
77. Grimme, S. Exploration of chemical compound, conformer, and reaction space with meta-dynamics simulations based on tight-binding quantum chemical calculations. *Journal chemical theory computation* **15**, 2847–2862 (2019).
78. Grimme, S. *et al.* Fully automated quantum-chemistry-based computation of spin–spin-coupled nuclear magnetic resonance spectra. *Angewandte Chemie International Edition* **56**, 14763–14769 (2017).
79. https://github.com/yangkevin2/coronavirus_data/tree/master/data. Accessed: 2020-07-06.
80. <https://www.aicures.mit.edu/data> (2020). Accessed: 2020-05-22.
81. Ellinger, B. *et al.* Identification of inhibitors of sars-cov-2 in-vitro cellular toxicity in human (caco-2) cells using a large scale drug repurposing collection. *Research Square preprint: 10.21203/rs.3.rs-23951/v1* (2020).
82. Touret, F. *et al.* In vitro screening of a fda approved chemical library reveals potential inhibitors of sars-cov-2 replication. *BioRxiv* (2020).
83. Main protease structure and xchem fragment screen. <https://www.diamond.ac.uk/covid-19/for-scientists/Main-protease-structure-and-XChem.html>.
84. Tokars, V. & Mesecar, A. QFRET-based primary biochemical high throughput screening assay to identify inhibitors of the SARS coronavirus 3C-like Protease (3CLPro). <https://pubchem.ncbi.nlm.nih.gov/bioassay/1706>.
85. Zampieri, M., Zimmermann, M., Claassen, M. & Sauer, U. Nontargeted metabolomics reveals the multilevel response to antibiotic perturbations. *Cell reports* **19**, 1214–1228 (2017).
86. Geom: Energy-annotated molecular conformations. <https://github.com/learningmatter-mit/geom>.
87. Halgren, T. A. Merck molecular force field. I. Basis, form, scope, parameterization, and performance of MMFF94. *Journal computational chemistry* **17**, 490–519 (1996).
88. Neese, F. The ORCA program system. *Wiley Interdisciplinary Reviews: Computational Molecular Science* **2**, 73–78 (2012).
89. Neese, F. Software update: the ORCA program system, version 4.0. *Wiley Interdisciplinary Reviews: Computational Molecular Science* **8**, e1327 (2018).
90. Kim, Y. & Kim, W. Y. Universal structure conversion method for organic molecules: from atomic connectivity to three-dimensional geometry. *Bulletin Korean Chemical Society* **36**, 1769–1777 (2015).
91. Converts and [sic] xyz file to an RDKit mol object. <https://github.com/jensengroup/xyz2mol>. Accessed: 2020-04-12.
92. Axelrod, S. & Gomez-Bombarelli, R. Molecular machine learning with conformer ensembles. *arXiv preprint arXiv:2012.08452* (2020).

93. Xu, M., Luo, S., Bengio, Y., Peng, J. & Tang, J. Learning neural generative dynamics for molecular conformation generation. In *International Conference on Learning Representations* (2021).
94. Frederick, K. K., Marlow, M. S., Valentine, K. G. & Wand, A. J. Conformational entropy in molecular recognition by proteins. *Nature* **448**, 325–329 (2007).
95. Murphy, K. P. *Machine learning: a probabilistic perspective* (MIT press, 2012).
96. Breiman, L. Random forests. *Machine learning* **45**, 5–32 (2001).
97. Rogers, D. & Hahn, M. Extended-connectivity fingerprints. *Journal chemical information modeling* **50**, 742–754 (2010).
98. Gilmer, J., Schoenholz, S. S., Riley, P. F., Vinyals, O. & Dahl, G. E. Neural message passing for quantum chemistry. In *Proceedings of the 34th International Conference on Machine Learning-Volume 70*, 1263–1272 (JMLR. org, 2017).
99. Yang, K. *et al.* Analyzing learned molecular representations for property prediction. *Journal chemical information modeling* **59**, 3370–3388 (2019).
100. Schütt, K. T., Sauceda, H. E., Kindermans, P.-J., Tkatchenko, A. & Müller, K.-R. SchNet—A deep learning architecture for molecules and materials. *The Journal Chemical Physics* **148**, 241722 (2018).
101. Schütt, K. *et al.* SchNet: A continuous-filter convolutional neural network for modeling quantum interactions. In *Advances in neural information processing systems*, 991–1001 (2017).
102. Axelrod, S. & Gomez-Bombarelli, R. Conformer models and training datasets. <https://doi.org/10.7910/DVN/N4VLQL> (2021).
103. Distributed Asynchronous Hyperparameter Optimization in Python. <https://github.com/hyperopt/hyperopt>. Accessed: 2020-09-03.
104. Neural Force Field. <https://github.com/learningmatter-mit/NeuralForceField>.
105. Axelrod, S. & Gomez-Bombarelli, R. GEOM. <https://doi.org/10.7910/DVN/JNGTDF> (2021).
106. MessagePack serializer implementation for Python. <https://github.com/msgpack/msgpack-python>. Accessed: 2020-05-02.
107. Becke, A. D. Density-functional exchange-energy approximation with correct asymptotic behavior. *Physical review A* **38**, 3098 (1988).
108. Perdew, J. P. Density-functional approximation for the correlation energy of the inhomogeneous electron gas. *Physical Review B* **33**, 8822 (1986).
109. Grimme, S., Antony, J., Ehrlich, S. & Krieg, H. A consistent and accurate ab initio parametrization of density functional dispersion correction (DFT-D) for the 94 elements H-Pu. *The Journal chemical physics* **132**, 154104 (2010).
110. Weigend, F. & Ahlrichs, R. Balanced basis sets of split valence, triple zeta valence and quadruple zeta valence quality for H to Rn: Design and assessment of accuracy. *Physical Chemistry Chemical Physics* **7**, 3297–3305 (2005).
111. Chai, J.-D. & Head-Gordon, M. Systematic optimization of long-range corrected hybrid density functionals. *The Journal chemical physics* **128**, 084106 (2008).
112. Melander, M., Laasonen, K. & Jonsson, H. Removing external degrees of freedom from transition-state search methods using quaternions. *Journal chemical theory computation* **11**, 1055–1062 (2015).
113. Crest. <https://github.com/grimme-lab/crest/releases>.
114. Xtb. <https://github.com/grimme-lab/xtb/releases>.

Acknowledgements

The authors thank the XSEDE COVID-19 HPC Consortium, project CHE200039, for compute time. NASA Advanced Supercomputing (NAS) Division and LBNL National Energy Research Scientific Computing Center (NERSC), MIT Engaging cluster, Harvard Cannon cluster, and MIT Lincoln Lab Supercloud clusters are gratefully acknowledged for computational resources and support. We kindly thank Professor Eugene Shakhnovich (Harvard) for enlightening discussions. The authors also thank Christopher E. Henze (NASA) and Shane Canon and Laurie Stephey (NERSC) for technical discussions and computational support, MIT AI Cures (<https://www.aicures.mit.edu/>) for molecular datasets and Wujie Wang, Daniel Schwalbe Koda, Shi Jun Ang (MIT DMSE) for scientific discussions and access to computer code. Financial support from DARPA (Award HR00111920025) and MIT-IBM Watson AI Lab is acknowledged.

Author contributions statement

R.G.B. conceived the project and S.A. performed the calculations. Both authors wrote and revised the manuscript.

Competing interests

The authors declare no competing interests.

Figures & Tables

CC(C)OC(=O)CCC/C=C\C[C@H]1[C@@H](O)C[C@@H](O)[C@@H]1CC[C@@H](O)CCc1ccccc1

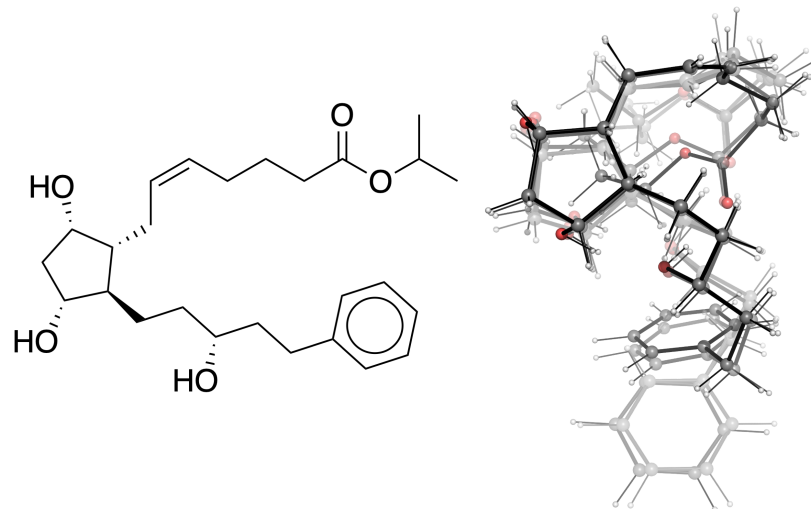


Figure 1. Molecular representations of the latanoprost molecule. *top* SMILES string. *left* Stereochemical formula with edge features, including wedges for in- and out-of-plane bonds, and a double line for *cis* isomerism. *right* Overlay of conformers. Higher transparency corresponds to lower statistical weight.

Drug dataset (N=304,466)			
	Mean	Standard deviation	Maximum
Number of atoms	44.4	11.3	181
Number of heavy atoms	24.9	5.7	91
Molecular weight (amu)	355.4	80.4	1549.7
Number of rotatable bonds	6.5	3.0	53
Stereochemistry (specified)	45,712	-	-
Stereochemistry (all)	83,326	-	-
QM9 dataset (N=133,258)			
	Mean	Standard deviation	Maximum
Number of atoms	18.0	3.0	29
Number of heavy atoms	8.8	0.51	9
Molecular weight (amu)	122.7	7.6	152.0
Number of rotatable bonds	2.2	1.6	8
Stereochemistry (specified)	95,734	-	-
Stereochemistry (all)	95,734	-	-

Table 1. Molecular descriptor statistics for the drug-like molecules and the QM9 molecules in the GEOM dataset.

Target	Number of Species	Hits	Sources
SARS-CoV-2	5,832	101	81,82
SARS-CoV-2 3CL protease	817	78	83
SARS-CoV 3CL protease	289,808	447	84
SARS-CoV PL protease	232,708	696	64,65
<i>E. Coli</i>	2,186	111	3,85
<i>Pseudomonas aeruginosa</i>	1,968	48	80

Table 2. Experimental data available for species in the GEOM dataset.

Drug dataset			
	Mean	Std. deviation	Maximum
S (cal/mol K)	8.2	2.6	16.8
$-G$ (kcal/mol)	2.4	0.8	5.0
$\langle E \rangle$ (kcal/mol)	0.4	0.2	2.4
Conformers	102.6	159.1	7,451
QM9 dataset			
	Mean	Std. deviation	Maximum
S (cal/mol K)	3.9	2.8	14.2
$-G$ (kcal/mol)	1.2	0.8	4.2
$\langle E \rangle$ (kcal/mol)	0.2	0.2	2.2
Conformers	13.5	42.2	1,101

Figure 2. CREST-based statistics for the drug and QM9 datasets.

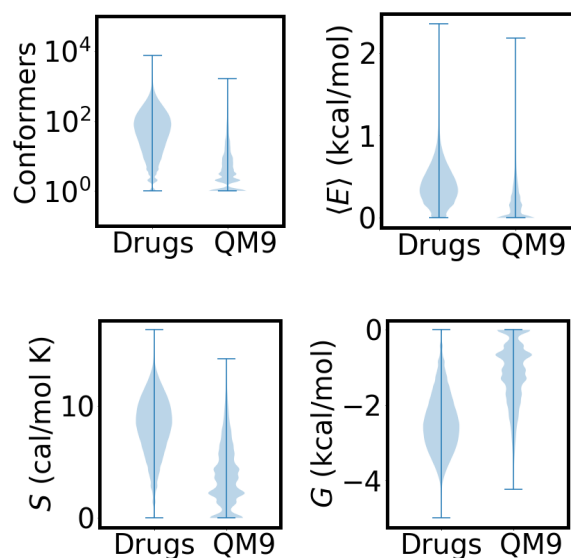


Figure 3. Violin plots of CREST-based statistics for the drug and QM9 datasets.

Model	G (kcal/mol)	$\langle E \rangle$ (kcal/mol)	$\ln(\text{unique conformers})$
Random Forest	0.406	0.166	0.763
KRR	0.289	0.131	0.484
FFNN	0.274	0.119	0.455
ChemProp	0.225	0.110	0.380
SchNetFeatures	0.203	0.113	0.363

Table 3. Prediction MAE for three conformer-related properties. Models were trained and tested on the drug dataset.

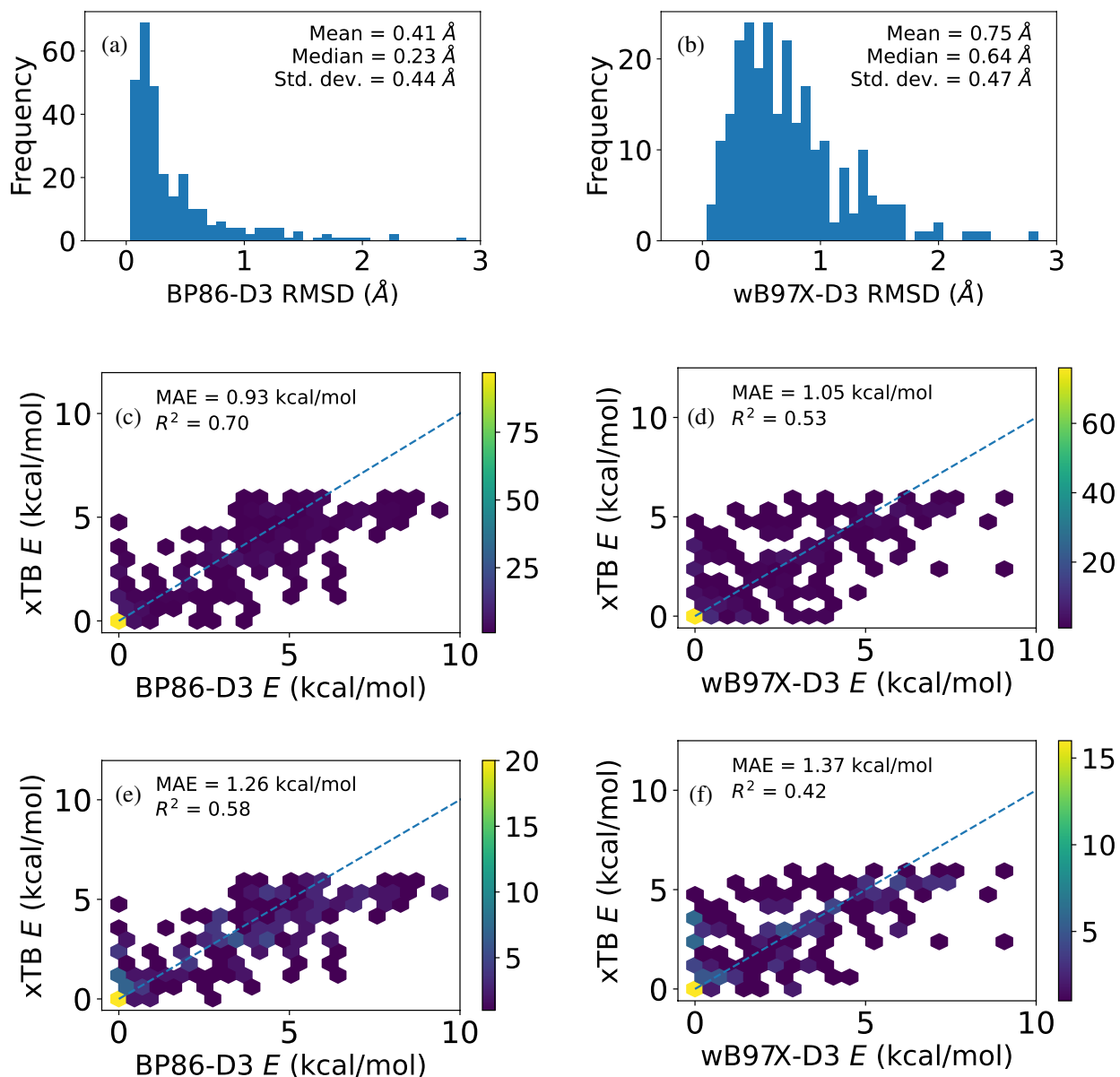


Figure 4. Comparison of geometries and energies calculated at different levels of theory. (a) RMSD between conformers optimized with xTB and with BP86-D3/def2-SVP. (b) As in (a), but with wb97X-D3/def2-TZVP. (c) Energy E of conformers optimized with xTB and with BP86-D3/def2-SVP. E is defined with respect to the conformer of lowest energy calculated at the same level of theory. The dashed line shows the ideal perfect correlation. (d) As in (c), but with wb97X-D3/def2-TZVP. Panels (e) and (f) are as in (d) and (c), respectively, but excluding the lowest energy xTB geometries.